Chemistry Europe
European Chemical Societies Publishing

WILEY VCH

Excellence in Chemistry Research

Announcing our new flagship journal

- Gold Open Access
- Publishing charges waived
- Preprints welcome
- Edited by active scientists

Meet the Editors of *ChemistryEurope*

Luisa De Cola
Università degli Studi di Milano Statale, Italy

Ive Hermans
University of Wisconsin-Madison, USA

Ken Tanaka
Tokyo Institute of Technology, Japan

Chemistry–A European Journal
Research Article
doi.org/10.1002/chem.202301389
Chemistry Europe
European Chemical Societies Publishing
www.chemeurj.org

Hot Paper

Organo-Functionalized Lacunary Double Cubane-Type Oxometallates: Synthesis, Structure, and Properties of $[(M^{II}Cl)_2(V^{IV}O)_2\{((HOCH_2CH_2)(H)N(CH_2CH_2O))(HN(CH_2CH_2O)_2)\}_2]$ (M = Co, Zn)

Damola T. Shuaib,[a] LaSalle Swenson,[a] James A. Kaduk,[a] Tieyan Chang,[b] Yu-Sheng Chen,[b] James McNeely,[c] and M. Ishaque Khan*[a]

Organofunctionalized tetranuclear clusters $[(M^{II}Cl)_2(V^{IV}O)_2\{((HOCH_2CH_2)(H)N(CH_2CH_2O))(HN(CH_2CH_2O)_2)\}_2]$ (**1**, M = Co, **2**: M = Zn) containing an unprecedented oxometallacyclic $\{M_2V_2Cl_2N_4O_8\}$ (M = Co, Zn) framework have been prepared by solvothermal reactions. The new oxo-alkoxide compounds were fully characterized by spectroscopic methods, magnetic susceptibility measurement, DFT and ab initio computational methods, and complete single-crystal X-ray diffraction structure analysis. The isostructural clusters are formed of edge-sharing octahedral $\{VO_5N\}$ and trigonal bipyramidal $\{MO_3NCl\}$ units. Diethanolamine ligates the bimetallic lacunary double cubane core of **1** and **2** in an unusual two-mode fashion, unobserved previously. In the crystalline state, the clusters of **1** and **2** are joined by hydrogen bonds to form a three-dimensional network structure. Magnetic susceptibility data indicate weakly antiferromagnetic interactions between the vanadium centers [J_{iso}-(V^{IV}–V^{IV}) = −5.4(**1**); −3.9(**2**) cm^{-1}], and inequivalent antiferromagnetic interactions between the cobalt and vanadium centers [J_{iso} (V^{IV}–Co^{II}) = −12.6 and −7.5 cm^{-1}] contained in **1**.

Introduction

Transition metal-oxide clusters or polyoxometalates (POMs) are formed mainly by V, Mo, and W.[1] The prototypical POM is completely inorganic, composed of metal cations (e.g., V^{V}, Mo^{VI}, W^{VI}) bridged by oxide ions. POMs have been applied in a range of technical areas, including acid and (photo-)redox catalysis,[2] biomedicine[3] and magnetism.[4] Energy storage and conversion applications include water splitting,[5] CO_2 reduction,[6] solar energy conversion,[7] Faradaic supercapacitors,[8] and ion-insertion[9] and redox flow[10] batteries. Technical applications are facilitated by the incorporation of POMs as active constituents in a variety of metal–organic frameworks[11] and supramolecular assemblies.[2b,11,12] The most common POM metal nuclearites fall in the range 6–18. Polyoxovanadates are often mixed valence (e.g., V^{IV}–V^{V}) species containing d^1 ions (V^{IV}) and are normally investigated for magnetic properties,[4] including superexchange interactions between the single-atom-bridged metal centers. Low nuclearity (ca. <6) polyoxovanadates are commonly obtained as organo-functionalized species by self-assembly through the addition of organic ligands to POM precursors.[13] Reports of organo-functionalized vanadium tetrametalates $([V_4O_nL_z])^{m-}$[14] and of their heteronuclear counterparts $([V_xM_{4-x}O_nL_z])^{m-}$[14e,15] are sparse. Here we report two bimetallic, tetranuclear, organo-functionalized, oxo-alkoxide clusters, $[(M^{II}Cl)_2(V^{IV}O)_2\{((HOCH_2CH_2)(H)N(CH_2CH_2O))(HN(CH_2CH_2O)_2)\}_2]$ (**1**, M=Co; **2**, M=Zn) containing the unprecedented oxometallacyclic $\{M_2V_2Cl_2N_4O_8\}$ (M=Co, Zn) framework and incorporating diethanolamine (DEA) ligands via distinct metal–ligand bonding modes. Such clusters of definite topology can be considered model systems in molecular magnetism and for the study of spin coupling.[4a,14g] The new V^{IV} clusters contain coupled d^1 (**1** and **2**) and d^7 (**1**) spin centers. (Photo-)redox active POM show strong charge-transfer bands in the UV.[1b] Multiple electronic transitions are indicated by broad UV–vis absorption bands in each compound. The complex electronic and magnetic structure of these low metal-nuclearity clusters makes them both theoretically and technologically intriguing chemical species. To the best of our knowledge, no mixed-metal tetranuclear clusters containing the Co–V or Zn–V combination have been reported.

Results and Discussion

Synthesis and structure

The organofunctionalized clusters **1** and **2** were synthesized by solvothermal methods (see the Supporting Information for synthesis procedure) in 49 and 58% yields, respectively. X-ray diffraction crystal structure analysis revealed that **1** and **2** are molecularly and crystallographically isomorphous. Crystallo-

[a] D. T. Shuaib, L. Swenson, J. A. Kaduk, Prof. M. I. Khan
Department of Chemistry, Illinois Institute of Technology
Chicago, IL 60616 (USA)
E-mail: khan@iit.edu
[b] T. Chang, Y.-S. Chen
ChemMatCARS, The University of Chicago
Lemont, IL 60439 (USA)
[c] J. McNeely
Department of Chemistry, Boston University
Boston, MA 02215 (USA)

Supporting information for this article is available on the WWW under https://doi.org/10.1002/chem.202301389

graphic data is shown in Table 1. In each case, the structure is composed of a novel metallocyclic core $\{M_2V_2Cl_2N_4O_8\}$ (M=Co, Zn) incorporating four DEA ligands in two distinct ligating modes (Figure 1). The core of each cluster consists of two distorted $\{VO_5N\}$ octahedra sharing a single edge; and two distorted $\{MO_3NCl\}$ trigonal bipyramidal units, each sharing an edge with both vanadium octahedra (Figure 1b). Each vanadium octahedra contains the nitrogen atom (V–N, 2.138 Å, **1**; 2.121 Å, **2**) and four bridging oxygen atoms of the $\{HN(CH_2–CH_2–O)_2\}$ ligands; and a terminal oxygen atom (V=O_t; V–O, 1.610 Å, **1**; 1.593 Å, **2**), which is a structural feature characteristic of polyoxoanions. The distorted trigonal bipyramidal geometry around the M (M=Co, Zn) centers is defined by a peripheral terminal chlorine atom (M–Cl, 2.282 Å, **1**; 2.236 Å, **2**); each M is also bound to the nitrogen atom (M–N, 2.172 Å, **1**; 2.127 Å, **2**) and a single oxygen atom of the $\{HN(CH_2–CH_2–O)(CH_2–CH_2–OH)\}$ ligand (Figure S1 in the Supporting Information). The inorganic core may be described as composed of two face-sharing Cubans, each missing a vertex. The coordination geometries of cobalt and vanadium and orthogonal views of the cluster compound in **1** with space-filled representations of cobalt and vanadium are shown in Figure 2.

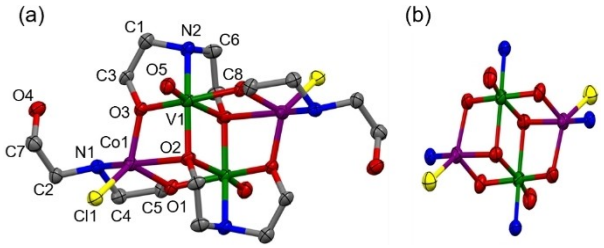

Figure 1. Ball-and-stick representation of the bimetallic tetrametalate clusters of a) $[(Co^{II}Cl)_2(V^{IV}O)_2\{((HOCH_2CH_2)(H)N(CH_2CH_2O))(HN(CH_2CH_2O)_2)\}_2]$ (**1**) and b) $([(Zn^{II}Cl)_2(V^{IV}O)_2\{((HOCH_2CH_2)(H)N(CH_2CH_2O))(HN(CH_2CH_2O)_2)\}_2]$ (**2**); Figure S1a). The tetrametalate core $\{Co_2V_2Cl_2N_4O_8\}$ of **1** ($\{Zn_2V_2Cl_2N_4O_8\}$; Figure S1b). The displayed thermal ellipsoids represent 50% displacement probability. Hydrogen atoms are omitted for clarity. Selected bond lengths [Å] and angles [°]: **1**; Co1–O1 1.933(3), Co1–O3 1.934(3), Co1–N1 2.172(3), Co1–Cl1 2.282(11), V1–O2 2.011(3), V1–O3 1.979(3), V1–O5 1.601(3), V1–N2 2.138(3), Co1–V1 3.178, Cl1–Co1–N1 100.160(9), Cl1–Co1–O1 124.810(9), Cl1–Co1–O3 123.300(9).

Table 1. X-ray crystal data of compounds **1** and **2**.

Crystal data	1	2
CCDC	2081072	2142846
Molecular formula	$C_{16}H_{38}Cl_2Co_2N_4O_{10}V_2$	$C_{16}H_{38}Cl_2Zn_2N_4O_{10}V_2$
M_r [g/mol]	737.14	750.02
Crystal system	monoclinic	monoclinic
space group	$P2_1/n$	$P2_1/n$
T [K]	295	100
a, b, c [Å]	9.808(3), 13.142(4), 11.252(3)	9.7379(19) 12.947(8) 11.140(7)
β [°]	112.76(10)	112.76(3)
V [Å^3]	1337.55(7)	1295.17(5)
Z	4	4
Radiation type	synchrotron, $\lambda = 0.8854$ Å	synchrotron, $\lambda = 0.41328$ Å
μ [mm^{-1}]	3.94	0.63
ρ_{calcd} [g cm^{-3}]	1.83	1.92
Crystal size [mm]	0.024×0.018×0.013	0.15×0.05×0.05
Data collection		
Diffractometer	Bruker D8 goniometer	Bruker D8 goniometer
Absorption correction	multi-scan, *SADABS 2016/2*	multi-scan, *SADABS 2016/2*
T_{min}, T_{max}	0.683, 0.746	0.911, 0.969
No. of measured, independent and observed [$I > 2\sigma(I)$] reflections	7781, 1207, 1122	18966, 4411, 2630
R_{int}	0.068	0.130
(sin $\theta/\lambda)_{max}$ [Å^{-1}]	0.527	0.760
Refinement		
[a] $R[F^2 > 2\sigma(F^2)]$, [b] $wR(F^2)$, S	0.029, 0.083, 1.120	0.0636, 0.154, 0.890
data/restraints/parameters	1207/0/165	4411/0/165
H-atom treatment	H-atom parameters constrained	H-atom parameters constrained
largest diff. peak and hole [e Å^{-3}]	0.37, −0.39	1.10, −0.80

[a] $R1 = \Sigma||F_o|-|F_c||/\Sigma|F_o|$. [b] $wR2 = [\Sigma[w(F_o^2-F_c^2)^2]/\Sigma[w(F_o^2)^2]]^{1/2}$.

The isostructural clusters **1** and **2** crystallize in the monoclinic space group $P2_1/n$. In the crystalline state, the clusters are joined by hydrogen bonds to form a 3D network structure (Figures 3 and S3). Each secondary amine ligand of M (M=Co, Zn) acts as a (hydrogen) donor to a hydroxy group oxygen of a neighboring cluster to form a hydrogen bond (N1–H1C···O4). Each chlorine atom acts as a bifurcate hydrogen acceptor, accepting a hydrogen atom from a secondary amine ligand of V (N2–H2 C···Cl1) on a neighboring cluster, while also

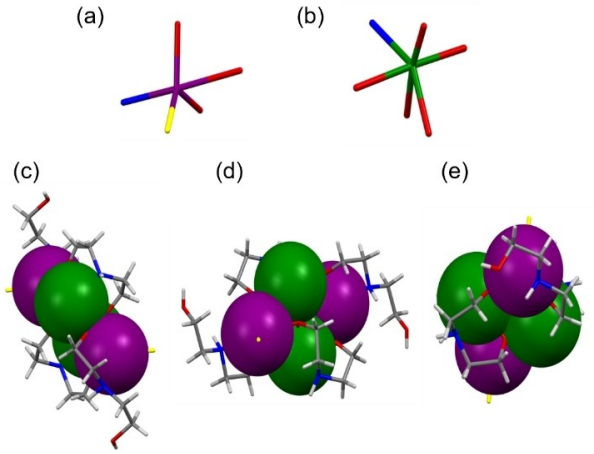

Figure 2. Capped-stick representations of a) the distorted trigonal bipyramidal cobalt coordination sphere and b) the distorted octahedral vanadium coordination sphere in $[(Co^{II}Cl)_2(V^{IV}O)_2\{((HOCH_2CH_2)(H)N(CH_2CH_2O))(HN(CH_2CH_2O)_2)\}_2]$ (**1**) shown along the crystallographic *b*-axis. c)–e) Orthogonal views of a cluster of compound **1** with space-filling representations of cobalt and vanadium. Color code: Co = purple, V = green, Cl = yellow, N = blue, O = red, C = gray, H = white. ($[(Zn^{II}Cl)_2(V^{IV}O)_2\{((HOCH_2CH_2)(H)N(CH_2CH_2O))(HN(CH_2CH_2O)_2)\}_2]$ (**2**); Figure S2).

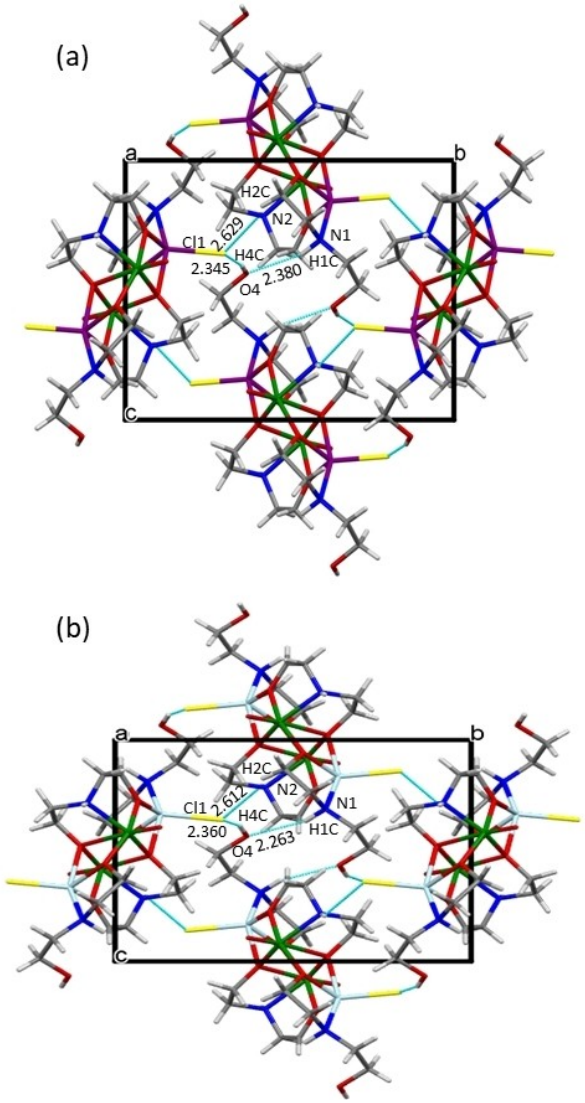

Figure 3. Stick representation of the unit cell content in the crystals of a) **1** and b) **2** viewed along the *a*-axis. Intercluster hydrogen bonds are indicated in turquoise and hydrogen bond distances [Å] are shown adjacent. Color code: Co = purple, V = green, Cl = yellow, N = blue, O = red, C = gray, H = white.

accepting a hydroxy group hydrogen (O4–H4C···Cl1) on a separate neighboring cluster. In this way each nucleophilic chlorine atom maximizes its interaction with positive charge centers. The O4–H4C···Cl1 and N1–H1C···O4 hydrogen bonds are interconnected through the σ-bond of the shared hydroxy group (Cl1···H4C–O4···H1C–N1). Each cluster is linked to six other clusters through twelve hydrogen bonds. The hydrogen-bonding motif observed in the condensed state shows that the peripheral nucleophilic chlorine atoms of distributed clusters can interact with positive charge centers. In analogy to Type III POMs, which contain nucleophilic terminal oxygen atoms, the terminal chlorine atoms of **1** and **2** should coordinate a variety of transition metals,[16] facilitating (electro-)catalytic activity and the formation of coordination polymers. Much of the application scope of active clusters relies on cluster heterogenation, often through electrostatic cluster-support interactions.[17] The chemical topology of the clusters **1** and **2** anticipates facile heterogenation through soft chemical methods.

Characterization

The infrared absorption spectra of **1** and **2** (Figures 4 and S4) contain bands associated with the oxometallate core and the DEA ligands. The likeness of the spectra is consistent with isostructural molecules differing only in the identity of a single atomic constituent. Typical IR absorption spectra of polyoxometalates contain strong bands associated with stretching modes of the terminal metal-oxygen bond ($M{=}O_t$), and weaker bands associated with bridging oxygen ($M{-}O_b{-}M$) vibrational modes. Band assignments are facilitated by spectral comparisons to previously studied DEA[18] and triethanolamine (TEA)[19] functionalized hexavanadate structures containing vanadium coordination octahedra like that observed in **1** and **2**. The strong band at around 958 cm^{-1} is attributed to the symmetric stretch of the terminal vanadium-oxygen bond ($\nu_{sym}V{=}O_t$). Multiple bands associated with ($V{-}O_b{-}V$) vibrational modes are expected and observed below about 800 cm^{-1}. Multiple bands associated with DEA functionalization are expected and observed in the 1000–1500 cm^{-1} range. Two distinct N–H stretching bands, corresponding to the vanadium and cobalt metal centers in **1** (V^{IV}–N–H and Co^{II}–N–H) and the vanadium and zinc metal centers in **2** (V^{IV}–N–H and Zn–N–H), are present in the respective spectra (see Figure S5 and associated discussion).

Comparison of the IR spectrum of **1** to $[NaV^{IV}_6O_6(OCH_2CH_2)_2NH)_6]^+$ (DEA-NaV_6)[18] reveals distinct bands at 989, 642, 562, and 497 cm^{-1}. Because terminal bonds are expected to have the most (nearly) pure stretching vibrations, and thus the highest IR absorption, we provisionally attribute the strong band at 989 cm^{-1} (Figure 4) to the symmetric stretch of the Co–Cl bond of the Co-centered polyhedra. Comparison of the IR spectrum of **2** to that of DEA–NaV_6 reveals distinct bands at 985, 639, 564, and 489 cm^{-1}. We provisionally attribute

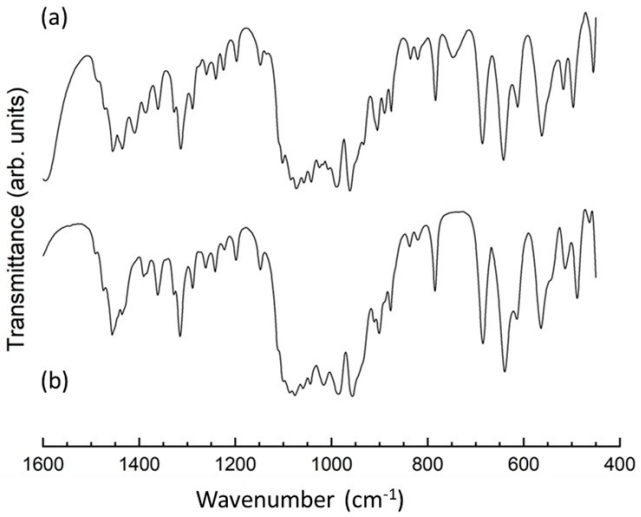

Figure 4. FTIR spectra of a) **1** and b) **2** in the 1600–450 cm^{-1} region.

the band at 985 cm^{-1} (Figure 4) to the symmetric stretch of the Zn–Cl bond of the Zn centered polyhedra.

Bond valence sum calculations[20] indicate metal oxidation states of V^{IV}, Co^{II}, and Zn^{II}, consistent with the X-ray structural data and charge balance requirements of **1** and **2**. Polyoxovanadates often occur as mixed valence (e.g., V^{IV}–V^{V}) species and exclusively reduced vanadium (V^{IV}) is often observed in low-nuclearity (e.g., $n \leq 6$) clusters functionalized with organic ligands, for example.[18,19,21] TGA profiles (Figures S6 and S7) of **1** and **2** overlay well until around 330 °C; decomposition initiates around 300 °C. This result is consistent with the identical nature of the organic moieties contained in each compound. **1** and **2** have comparable thermal stability to previously studied DEA- and TEA-functionalized hexavanadate compounds.[18–19] Divergence of the TGA profiles following initial decomposition implies that heteroatom identity (Co/Zn) has a marked effect on the chemical transformations accompanying thermal decomposition. (See the Supporting Information for a detailed analysis of the TGA.)

Both compounds are stable in air as confirmed by FTIR. Reflectance spectra covering the UV, visible and a portion of the near-IR range of compounds **1** and **2** are plotted as pseudo-absorbances (1-*R*) in Figure 5. Broad bands are present in the UV, vis and NIR ranges for both compounds. In POMs, UV bands are associated with charge transfer processes between terminal oxygen atoms and (usually) octahedral metal centers; these are present in the V^{IV} octahedra of **1** and **2**. The redox activity of certain POM species is attributable to this process.[1b] We previously found both UV and visible absorption bands in hexavanadate clusters containing V^{IV} coordination octahedra like those found in **1** and **2**.[18–19] The shape and breadth of the UV absorption bands suggests an additional contribution from M–Cl (M=Co, Zn) charge transfer processes. Visible bands are associated with d–d and intervalence transitions arising from reduced metal cations (e.g., V^{IV}).[22] In this regard we observe that compound **1**, containing (formally) $Co(d^7)$ has a broader visible absorption spectrum than compound **2**, which contains zinc with a (formally) full d-subshell. Thus the spectra are consistent with the structure and metal oxidation states of the compounds.

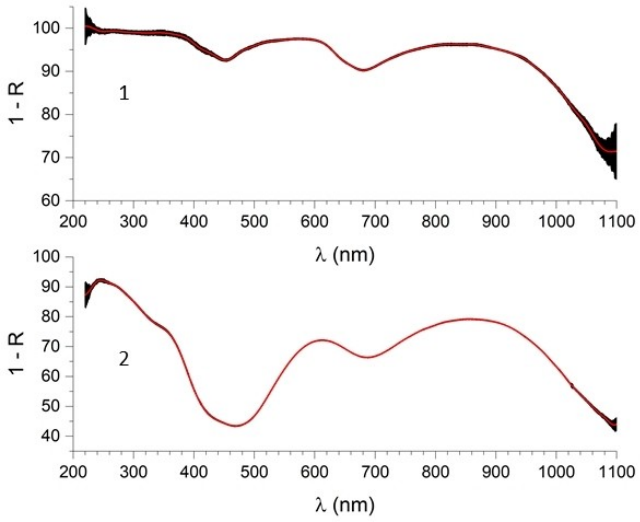

Figure 5. UV–Vis-NIR (220–1100 nm) reflectance spectra of **1** (top) and **2** (bottom). A reflectance fraction (*R*) was obtained by comparison to a reflectance standard, and pseudo absorption spectra were derived by subtracting *R* from unity (plotted). Error bands represent ± one standard deviation over 20 scans.

Magnetic properties

The magnetic susceptibilities of **1** and **2** are shown in Figure 6a. The exchange couplings are defined in Figure 6b, and axes systems for the V^{IV} and Co^{II} centers are found in Figure 6c. The susceptibility for **1** was successfully modeled (EasySpin[23]) with $g_{iso}^{V^{IV}} = 1.94$, $g_{x,y,z}^{Co^{II}} = 2.03,\ 2.57,\ 2.52$, $J_1 = -5.35\ cm^{-1}$, $J_2' = -12.58\ cm^{-1}$, $J_2'' = -7.48\ cm^{-1}$, $D^{Co^{II}} = 25.1\ cm^{-1}$, and $E/D = 0.04$. The spin Hamiltonian (SH) parameters were also reasonably reproduced with multi-reference NEVPT2 calculations (see the Supporting Information for details) performed with ORCA.[24] The computationally predicted parameters were $g_{iso}^{V^{IV}} = 1.96$, $g_{x,y,z}^{Co^{II}} = 2.02,\ 2.39,\ 2.34$, $J_1 = -1.39\ cm^{-1}$, $J_2' = -13.02\ cm^{-1}$, $J_2'' = -4.11\ cm^{-1}$, $D^{Co^{II}} = 39.1\ cm^{-1}$, and $E/D = 0.06$. Furthermore, these parameters can be predicted to be $g_{iso}^{V^{IV}} = 1.96$, $g_{x,y,z}^{Co^{II}} = 2.00,\ 2.42,\ 2.26$, $D^{Co^{II}} = 29.3\ cm^{-1}$, and $E/D = 0.24$ using ligand-field theory based on energies and spin–orbit coupling constants derived from ab-initio ligand field theory (AILFT). For **2**, the experimental/computational/LFT SH parameters were found to be $g_{x,y,z}^{V^{IV}} =$

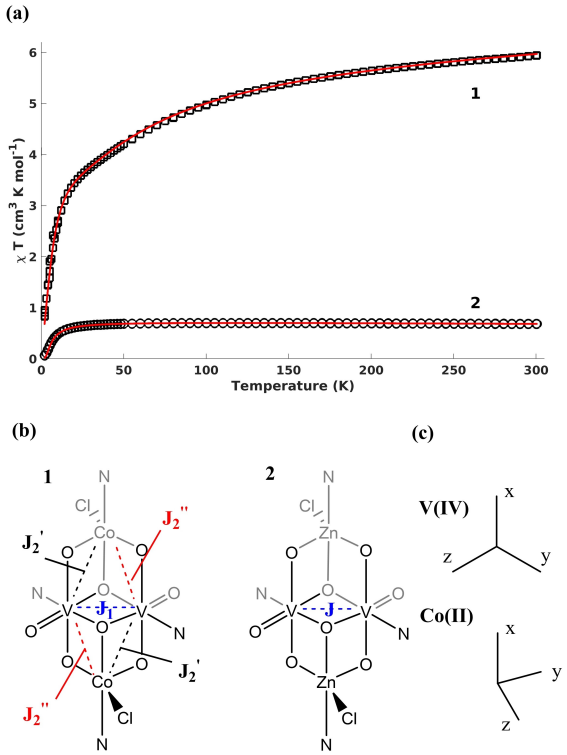

Figure 6. a) Temperature dependence of the χT product for **1** (·) and **2** (•) at 0.1 T. Fits with parameters shown in the text are in red. b) Definition of the exchange coupling constants used in this work. c) Coordinate systems used to describe the Co^{II} and V^{IV} centers.

1.98, 1.99, 2.00/1.93, 1.98, 1.98/1.92, 1.98, 1.98 and $J = -3.91/-1.9\ cm^{-1}$.

The isotropic *g* value extracted from the susceptibility is standard for V^{IV} centers in pseudo-octahedral environments. In particular, the value of 1.95 observed here agrees nicely with the EPR-derived value of 1.97 observed on a tetravanadate system by Plass.[25] The exchange couplings observed (and predicted) for both **1** and **2** are all antiferromagnetic.

The *anti*-coplanar orientation of the V^{IV} centers in these systems are qualitatively expected to favor weak antiferromagnetic interactions based on the structural features of the molecule. We observe that the V=O_t bonds are not purely coplanar with an O^{trans}–V–O_t angle of ±169.7 and ±170.4 for **1** and **2** respectively. We also observe that the V^{IV} $3d_{xy}$ orbitals are twisted as evidenced by the N–V–O–V torsions deviating from 180° by 20° and 19° for **1** and **2** respectively. These deformations result in non-zero overlap between the V^{IV} magnetic orbitals which is supported by the corresponding orbital overlaps of 0.015/0.017 observed for $\mathbf{1}^{Zn}$/**2** with broken symmetry PBE0/DKH-DEF2-QZVPP(V,Zn,Co)/DKH-DEF2-TZVP/DKH solutions, where $\mathbf{1}^{Zn}$ substitutes the Co^{II} centers with Zn^{II} centers. Our observed values for the V–V exchange interactions are similar to that observed by Lu et al. on an *anti*-coplanar V^{IV} dimer.[26] This work can also be compared with the work of Stuckart et al.,[27] who studied the magnetic exchange interactions between octahedral V^{IV} centers and square pyramidal V^{IV} centers through a WO_4^{2-} unit. Interestingly, they observed an antiferromagnetic exchange coupling of $-5.35\ cm^{-1}$, which is of similar magnitude to the value observed in this work. This highlights that the overlap between the $3d_{xy}$ in our systems are weak enough to dampen the exchange interaction to the degree that it makes the superexchange pathway nearly equivalent to WO_4^{2-} pathways. All of the interactions reported in this work and referenced for comparison are significantly below the values regularly observed for bis(μ-OH) bridged V^{IV} systems.[28]

The interactions between the Co^{II} centers and the V^{IV} centers in **1** are inequivalent as predicted from the experimental structure where the Co–V distances are 3.18 Å and 3.29 Å. It can also be observed that the superexchange pathway for the different exchange couplings (J_2', J_2'') are inequivalent as illustrated in Figure 7. Inspection of Figure 7 suggests that J_2' will be stronger than J_2'' due to the enhanced overlap between the V-$3d_{xy}$ orbital and the sp^2 hybridized μ2-O. Fraser et al. recently reported a Co/V Anderson wheel complex that likewise showed divergence of the exchange couplings between neighboring cobalt centers and adjacent edges on vanadium centers.[29]

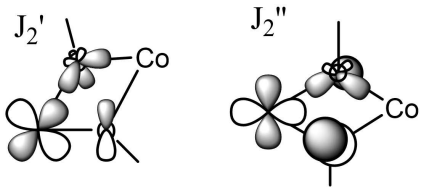

Figure 7. Qualitative illustration of inequivalent superexchange pathways for J_2' and J_2''.

Conclusions

In conclusion, we have prepared and fully characterized two isostructural organo-functionalized mixed-metal clusters $[(Co^{II}Cl)_2(V^{IV}O)_2\{((HOCH_2CH_2)(H)N(CH_2CH_2O))(HN(CH_2CH_2O)_2)\}_2]$ (**1**) and $[(Zn^{II}Cl)_2(V^{IV}O)_2\{((HOCH_2CH_2)(H)N(CH_2CH_2O))(HN(CH_2CH_2O)_2)\}_2]$ (**2**), which contain an unprecedented oxometallacyclic $\{M_2V_2Cl_2N_4O_8\}$(M=Co, Zn) framework incorporating diethanolamine ligands via two distinct metal-ligand bonding modes, previously unobserved. The clusters contain terminal oxygen and chlorine atoms and have UV–vis absorption spectra consistent with multiple UV charge-transfer processes. In **1**, there are four weakly coupled spin centers, where the isotropic exchange couplings are defined as J_1, J_2', and J_2''. These couplings are $J_1 = -5.4\ cm^{-1}$, $J_2' = -12.6\ cm^{-1}$, and $J_2'' = -7.5\ cm^{-1}$. The ground state multiplicity of **2** is an open-shell singlet with an isotropic exchange coupling of $-3.9\ cm^{-1}$. The vanadium centers are best described as a V^{IV} centers, and the cobalt centers are high-spin Co^{II} centers. Less orbital destabilization was observed due to weaker interaction of Cl^- ligand on Co than what was observed for O^{2-} ligand on V centers.

Experimental Section

Synthesis

$[(Co^{II}Cl)_2(V^{IV}O)_2\{((HOCH_2CH_2)(H)N(CH_2CH_2O))(HN(CH_2CH_2O)_2\}_2]$ (1): Tetrabutylammonium trihydrogendecavanadate hexahydrate $[(C_4H_9)_4N]_3[H_3V_{10}O_{28}]\cdot 6H_2O$ was synthesized according to a literature method.[30] Tetrabutylammonium trihydrogendecavanadate hexahydrate (0.095 g, 0.05 mmol), cobalt(II) chloride hexahydrate, $CoCl_2\cdot 6H_2O$ (Sigma–Aldrich, ACS grade; 0.126 g, 0.53 mmol) and diethanolamine, $HN(CH_2CH_2OH)_2$ (Fisher Chemical, Laboratory grade; 0.263 g, 2.49 mmol) were mixed in a 23 mL Teflon-lined Parr reaction vessel. The vessel was heated to 145 °C, held for 4 h at 145 °C, and then cooled to room temperature at the rate of ca. 5 °C h^{-1}. Three 3-mL portions of ethanol were added to the dark brown gelatinous product with gentle stirring. A solid product was obtained by filtration and dried under ambient conditions. The final product, in the form of purple crystals, was separated from a light brown co-product mechanically. The product yield was ca. 49% based on vanadium. Elemental analysis: calcd for $C_{16}H_{38}Cl_2Co_2N_4O_{10}V_2$: C 26.07, H 5.20, N 7.60; found: C 25.98, H 5.19, N 7.39.

$[(Zn^{II}Cl)_2(V^{IV}O)_2\{((HOCH_2CH_2)(H)N(CH_2CH_2O))(HN(CH_2CH_2O)_2\}_2]$ (2): Tetrabutylammonium trihydrogen decavanadate hexahydrate $[(C_4H_9)_4N]_3[H_3V_{10}O_{28}]\cdot 6H_2O$ (0.095 g, 0.05 mmol), zinc(II) chloride $ZnCl_2$ (0.072 g, 0.53 mmol) and diethanolamine $HN(CH_2CH_2OH)_2$ (0.263 g, 2.49 mmol) were mixed in a 23 mL Teflon-lined parr reaction vessel. The vessel was heated to 145 °C, held for 4 h at 145 °C, and then cooled to room temperature at rate of ca. 5 °C h^{-1}. Three 3-mL portions of ethanol were added to the dark brown gelatinous product with gentle stirring. A solid product was obtained by filtration and dried under ambient conditions. The final product, in the form of blue crystals, was separated from other solid material mechanically. The product yield was ca. 58% based on

vanadium. Elemental analysis: calcd for $C_{16}H_{38}Cl_2Zn_2N_4O_{10}V_2$: C 25.62, H 5.11, N 7.47; found: C 26.02, H 5.06, N 7.40.

Characterization: Infra-red spectra were recorded on a Perkin Elmer Spectrum 100 FTIR spectrometer. An Ocean Optics HR4000 spectrometer controlled by Ocean Optics Spectra Suite Spectrometer Operating Software was used to obtain reflectance spectra of powdered samples of **1** and **2**. In-house constructed dark chamber fitted with UV–Vis-NIR light source (Mikropack, DH-2000-BAL). Reflectance was measured against a Labsphere certified reflectance standard (USRS-99-010) and is reported as a pseudo-absorbance obtained by subtracting the reflectance (R) from unity. A Mettler Toledo TGA 2 SF/1100/735 thermogravimetric analyzer was used to obtain TGA profiles of **1** and **2** (N_2, 100 mL min^{-1}) at a heating rate of 5 °C min^{-1} in the 25–1000 °C temperature range. X-ray diffraction patterns were measured using a $Cu_{K\alpha}$ radiation source ($\lambda = 1.54$ Å) on a Bruker D2 Phaser spectrometer equipped with LynxEye linear position-sensitive detector. Data was collected in the 5–100° (2θ) range with a 0.03 2θ step and a 7.0 s/step dwell time. Single-crystal-based simulated X-ray powder diffraction patterns corresponded to the empirical X-ray powder diffraction patterns of each compound. Single crystal X-ray data were collected using synchrotron radiation (0.8854 Å; compound **2**; 0.41328 Å) at Advanced Photon Source (APS), Argonne National Laboratory (ANL). Crystals suitable for X-ray diffraction were mounted on a glass fiber and transferred to a Bruker D8 platform goniometer equipped with a PILATUS3 X 2 M (Si 1 mm) detector. Using APEX III software package, data were integrated using SAINT V8.38A and scaled with a multi-scan absorption correction.[31] The crystal was kept at 295 K (compound **2**; 100 K) during data collection. Using Olex2, the structure was solved with the XT structure solution program[32] using intrinsic phasing and refined with the XL refinement package[33] using Least Squares minimization. All non-hydrogen atoms were refined anisotropically.[34] Deposition Numbers 2081072 (for **1**) and 2142846 (for **2**) contain the supplementary crystallographic data for this paper. These data are provided free of charge by the joint Cambridge Crystallographic Data Centre and Fachinformationszentrum Karlsruhe Access Structures service.

Magnetic measurements: The magnetic moment vs. temperature was measured by superconducting quantum interference device (SQUID) magnetometer MPMS *XL* at the Center for Nanoscale Materials (CNM) at Advanced Photon Source (APS), Argonne National Laboratory. Both zero field cooling and field cooling was performed at a temperature range of 2–300 K under helium and liquid nitrogen to achieve an ultracool system under reciprocating sample option (RSO) at magnetic field $H = 1000$ Oe. All moments were corrected for diamagnetic susceptibilities using Pascal's constants.[35] In addition, a term was used in fitting that allowed for temperature independent paramagnetism. The magnetic susceptibility was fit with the Heisenberg, Dirac, Van-Vleck (HDVV) spin Hamiltonian from 8 to 300 K, with the spin Hamiltonians shown in Equations (S1) and (S2) for **1** and **2** respectively. See the Supporting Information for further details.

Computational methods: The ORCA electronic structure suite, version 5, was used for all calculations.[36] The highly efficient resolution of identity (RI) and "chain or spheres" (COSX) approximations for the Coulomb and Exchange integrals respectively were employed (RIJCOSX[37]). Grimme's D4[38] dispersion correction was applied for all geometry optimizations. The DEF2-TZVP[39] basis set was employed for all geometry optimizations, and single point calculations used the relativistically recontracted DKH-DEF2-QZVPP basis set for all transition metals, and the relativistically recontracted DKH-DEF2-TZVP basis set for all other atoms. An automatically generated auxiliary basis set[40] was used for all single-point evaluations, which is the so-called "AutoAux" technique in ORCA parlance. Single point calculations also employed the scalar relativistic DKH2[41] Hamiltonian, and picture change effects were included in the calculation of spin-orbit coupling. NBO calculations were performed with NBO 7.0.[42] All DFT calculations employed the PBE0[43] hybrid functional. Broken-symmetry (BS) solutions were obtained using the "FlipSpin" technique as implemented in ORCA. See the Supporting Information for further details.

Supporting Information

Further representations of compounds **1** and **2**; FTIR spectra; TGA profiles; observed and simulated PXRD patterns. Calculated bond valences. Additional references are also cited within the Supporting Information.[44–47]

Acknowledgements

Single crystal X-ray data were collected using synchrotron radiation at NSF's ChemMatCARS, Sector 15 at the Advanced Photon Source (APS), Argonne National Laboratory (ANL), which is supported by the Divisions of Chemistry (CHE) and Materials Research (DMR), National Science Foundation, under grant number NSF/CHE- 1834750. Use of Magnetic Properties Measurement System (MPMS) was supported by Center for Nanoscale Materials (CNM) (proposal number 76496). Work performed at the Advanced Photon Source and Center for Nanoscale Materials, both U.S. Department of Energy Office of Science User Facilities, was supported by the U.S. DOE, Office of Basic Energy Sciences, under Contract No. DE-AC02-06CH11357.

Conflict of Interests

The authors declare no conflict of interest.

Data Availability Statement

The data that support the findings of this study are available in the supplementary material of this article.

Keywords: cobalt · polyoxovanadate · superexchange · tetranuclear complexes · zinc

[1] a) Special thematic issue on polyoxometalates. C. L. Hill (Guest ed.), *Chem. Rev.* **1998**, *98*, 1–390; b) M. T. Pope, *Heteropoly and Isopoly Oxometalates*, Springer, Berlin, New York, **1983**.
[2] a) G. Marci, E. I. Garcia-Lopez, L. Palmisano, *Eur. J. Inorg. Chem.* **2014**, *2014*, 21–35; b) P. Mialane, C. Mellot-Draznieks, P. Gairola, M. Duguet, Y. Benseghir, O. Oms, A. Dolbecq, *Chem. Soc. Rev.* **2021**, *50*, 6152–6220; c) J. B. Moffat, *Metal-Oxygen Clusters: The Surface and Catalytic Properties of Heteropoly Oxometalates*, Kluwer, New York, **2001**; d) I. V. Kozhevnikov, *Catalysis by Polyoxometalates; Catalysts for Fine Chemical Synthesis 2*, Wiley, Chichester, **2002**.
[3] M. B. Colovic, M. Lackovic, J. Lalatovic, A. S. Mougharbel, U. Kortz, D. Z. Krsti, *Curr. Med. Chem.* **2020**, *27*, 362–379.
[4] a) J. M. Clemente-Juan, E. Coronado, A. Gaita-Arino, *Chem. Soc. Rev.* **2012**, *41*, 7464–7478; b) A. Muller, F. Peters, M. T. Pope, D. Gatteschi,

Chem. Rev. **1998**, *98*, 239–272; c) N. Suaud, Y. Masaro, E. Coronado, J. M. Clemente-Juan, N. Guihéry, *Eur. J. Inorg. Chem.* **2009**, *2009*, 5109–5114.
[5] a) Y. Shimoyama, N. Ogiwara, Z. W. Weng, S. Uchida, *J. Am. Chem. Soc.* **2022**, *144*, 2980–2986; b) A. Kar, L. Sharma, A. Kumar, A. Halder, C. P. Pradeep, *Eur. J. Inorg. Chem.* **2022**, *2022*, e202101031.
[6] a) Y. Benseghir, A. Sole-Daura, P. Mialane, J. Marrot, L. Dalecky, S. Bechu, M. Fregnaux, M. Gomez-Mingot, M. Fontecave, C. Mellot-Draznieks, A. Dolbecq, *ACS Catal.* **2022**, *12*, 453–464; b) M. Lu, M. Zhang, J. Liu, T. Y. Yu, J. N. Chang, L. J. Shang, S. L. Li, Y. Q. Lan, *J. Am. Chem. Soc.* **2022**, *144*, 1861–1871; c) C. Wang, C. Y. Zhu, M. Zhang, Y. Geng, Y. G. Li, Z. M. Su, *J. Mater. Chem. A* **2020**, *8*, 14807–14814.
[7] a) L. Chen, W. L. Chen, X. L. Wang, Y. G. Li, Z. M. Su, E. B. Wang, *Chem. Soc. Rev.* **2019**, *48*, 260–284; b) Y. Y. Dong, Y. L. Yang, L. L. Qiu, G. H. Dong, D. B. Xia, X. D. Liu, M. R. Li, R. Q. Fan, *ACS Appl. Energ. Mater.* **2019**, *2*, 4224–4233; c) Y. T. Gu, L. Chen, J. P. Li, L. Liu, W. L. Chen, D. Liu, E. B. Wang, *Chinese J. Inorg. Chem.* **2019**, *35*, 1905–1920.
[8] X. Wang, H. Li, J. F. Lin, C. Y. Wang, X. L. Wang, *Inorg. Chem.* **2021**, *60*, 19287–19296.
[9] a) X. Y. Jia, J. X. Wang, H. B. Hu, Y. F. Song, *Chem. Eur. J.* **2020**, *26*, 5257–5263; b) Q. Li, M. Q. Xu, T. Wang, H. J. Wang, J. W. Sun, J. Q. Sha, *Chem. Eur. J.* **2022**, *28*, e202200207; c) H. Yang, T. Song, L. Liu, A. Devadoss, F. Xia, H. Han, H. Park, W. Sigmund, K. Kwon, U. Paik, *J. Phys. Chem. C* **2013**, *117*, 17376–17381.
[10] a) F. Ai, Z. Y. Wang, N. C. Lai, Q. L. Zou, Z. J. Liang, Y. C. Lu, *Nat. Energy* **2022**, *7*, 417–426; b) M. Anjass, G. A. Lowe, C. Streb, *Angew. Chem. Int. Ed.* **2021**, *60*, 7522–7532; c) C. L. Peake, A. J. Kibler, G. N. Newton, D. A. Walsh, *ACS Appl. Energ. Mater.* **2021**, *4*, 8765–8773.
[11] J. L. Liu, M. Y. Huang, Z. Y. Hua, Y. Dong, Z. R. Feng, T. D. Sun, C. X. Chen, *ChemistrySelect* **2022**, *7*, e202200546.
[12] J. M. Cameron, G. Guillemot, T. Galambos, S. S. Amin, E. Hampson, K. M. Haidaraly, G. N. Newton, G. Izzet, *Chem. Soc. Rev.* **2022**, *51*, 293–328.
[13] a) A. Proust, B. Matt, R. Villanneau, G. Guillemot, P. Gouzerh, G. Izzet, *Chem. Soc. Rev.* **2012**, *41*, 7605–7622; b) A. Proust, R. Thouvenot, P. Gouzerh, *Chem. Commun.* **2008**, 1837–1852.
[14] a) S. L. Castro, Z. Sun, J. C. Bollinger, D. N. Hendrickson, G. Christou, *J. Chem. Soc. Chem. Commun.* **1995**, 2517–2518; b) D. D. Heinrich, K. Folting, W. E. Streib, J. C. Huffman, G. Christou, *J. Chem. Soc. Chem. Commun.* **1989**, 1411–1413; c) O. Nachtigall, A. Hagenbach, J. Wiecko, D. Lentz, U. Abram, J. Spandl, *Dalton Trans.* **2017**, *46*, 509–516; d) J. R. Rambo, J. C. Huffman, O. Eisenstein, G. Christou, *J. Am. Chem. Soc.* **1989**, *111*, 8027–8029; e) Y. Wang, M. Fukuda, S. Nikolaev, A. Miyake, K. J. Griffith, M. L. Nisbet, E. Hiralal, R. Gautier, B. L. Fisher, M. Tokunaga, M. Azuma, K. R. Poeppelmeier, *Inorg. Chem.* **2022**, *61*, 10234–10241; f) W. Plass, *Inorg. Chem.* **1997**, *36*, 2200–2205; g) M. J. Manos, A. J. Tasiopoulos, E. J. Tolis, N. Lalioti, J. D. Woollins, A. M. Z. Slawin, M. P. Sigalas, T. A. Kabanos, *Chem. Eur. J.* **2003**, *9*, 695–703; h) A. Neves, L. M. Rossi, A. J. Bortoluzzi, A. S. Mangrich, W. Haase, O. R. Nascimento, *Inorg. Chem. Commun.* **2002**, *5*, 418–421.
[15] a) O. Kahn, P. Tola, J. Galy, H. Coudanne, *J. Am. Chem. Soc.* **1978**, *100*, 3931–3933; b) O. Kahn, J. Galy, Y. Journaux, J. Jaud, I. Morgensternbadarau, *J. Am. Chem. Soc.* **1982**, *104*, 2165–2176.
[16] B. Fabre, C. Falaise, E. Cadot, *ACS Catal.* **2022**, *12*, 12055–12091.
[17] A. S. Cherevan, S. P. Nandan, I. Roger, R. Liu, C. Streb, D. Eder, *Adv. Sci.* **2020**, *7*, 1903511.
[18] M. I. Khan, Y. Zheng, H. Li, L. Swenson, A. Basha, R. J. Doedens, *Dalton Trans.* **2014**, *43*, 16509–16514.
[19] H. Li, L. Swenson, R. J. Doedens, M. I. Khan, *Dalton Trans.* **2016**, *45*, 16511–16518.
[20] I. D. Brown, *Structure and Bonding in Crystals*, Academic Press, New York, **1981**.
[21] M. I. Khan, S. Tabussum, R. J. Doedens, V. O. Golub, C. J. O'Connor, *Inorg. Chem.* **2004**, *43*, 5850–5859.
[22] G. M. Varga, E. Papaconstantinou, M. T. Pope, *Inorg. Chem.* **1970**, *9*, 662–667.
[23] S. Stoll, A. Schweiger, *J. Magn. Reson.* **2006**, *178*, 42–55.
[24] a) F. Neese, F. Wennmohs, U. Becker, C. Riplinger, *J. Chem. Phys.* **2020**, *152*, 224108; b) F. Neese, *Wiley Interdiscip. Rev.: Comput. Mol. Sci.* **2018**, *8*, e1327; c) F. Neese, *Wiley Interdiscip. Rev.: Comput. Mol. Sci.* **2012**, *2*, 73–78.
[25] W. Plass, *Eur. J. Inorg. Chem.* **1998**, *1998*, 799–805.
[26] H. Lu, R. Gautier, Z.-X. Li, W. Jie, Z. Liu, K. R. Poeppelmeier, *J. Solid State Chem.* **2013**, *200*, 105–109.
[27] M. Stuckart, N. V. Izarova, M. Glöß, J. Klose, C. Schmitz-Antoniak, P. Kögerler, B. Kersting, K. Y. Monakhov, *Inorg. Chem.* **2021**, *60*, 8437–8441.
[28] K. Wieghardt, U. Bossek, K. Volckmar, W. Swiridoff, J. Weiss, *Inorg. Chem.* **1984**, *23*, 1387–1389.
[29] H. W. L. Fraser, E. H. Payne, A. Sarkar, L. R. B. Wilson, D. Mitcov, G. S. Nichol, G. Rajaraman, S. Piligkos, E. K. Brechin, *Dalton Trans.* **2021**, *50*, 12495–12501.
[30] W. G. Klemperer, O. M. Yaghi, *Inorg. Synth.* **1990**, *27*, 83.
[31] a) *SHELXTL* Version 2018/3; Bruker-AXS: Madison, Wisconsin, USA; b) SADABS 2016/2; Bruker AXS: Madison, Wisconsin, USA.
[32] G. M. Sheldrick, *Acta Crystallogr. Sect. A Found. Adv.* **2015**, *71*, 3–8.
[33] G. M. Sheldrick, *Acta Crystallogr. Sect. A Found. Crystallogr.* **2008**, *64*, 112–122.
[34] a) O. V. Dolomanov, L. J. Bourhis, R. J. Gildea, J. A. K. Howard, H. J. Puschmann, *Appl. Cryst.* **2009**, *42*, 339–341; b) *PLATON/SQUEEZE*; A. L. Spek, University of Utrecht (The Netherlands), **2011**.
[35] G. A. Bain, J. F. Berry, *J. Chem. Educ.* **2008**, *85*, 532.
[36] a) F. Neese, *Wiley Interdiscip. Rev.: Comput. Mol. Sci.* **2012**, *2*, 73–78; b) F. Neese, *Wiley Interdiscip. Rev.: Comput. Mol. Sci.* **2018**, *8*, e1327; c) F. Neese, F. Wennmohs, U. Becker, C. Riplinger, *J. Chem. Phys.* **2020**, *152*, 224108.
[37] a) F. Neese, *J. Comput. Chem.* **2003**, *24*, 1740–1747; b) F. Neese, F. Wennmohs, A. Hansen, U. Becker, *Chem. Phys.* **2009**, *356*, 98–109; c) S. Kossmann, F. Neese, *Chem. Phys. Lett.* **2009**, *481*, 240–243; d) R. Izsák, F. Neese, *J. Chem. Phys.* **2011**, *135*, 144105; e) D. Ganyushin, N. Gilka, P. R. Taylor, C. M. Marian, F. Neese, *J. Chem. Phys.* **2010**, *132*, 144111.
[38] a) E. Caldeweyher, C. Bannwarth, S. Grimme, *J. Chem. Phys.* **2017**, *147*, 034112; b) E. Caldeweyher, S. Ehlert, A. Hansen, H. Neugebauer, S. Spicher, C. Bannwarth, S. Grimme, *J. Chem. Phys.* **2019**, *150*, 154122.
[39] a) F. Weigend, R. Ahlrichs, *Phys. Chem. Chem. Phys.* **2005**, *7*, 3297–3305; b) F. Weigend, *Phys. Chem. Chem. Phys.* **2006**, *8*, 1057–1065.
[40] G. L. Stoychev, A. A. Auer, F. Neese, *J. Chem. Theory Comput.* **2017**, *13*, 554–562.
[41] a) B. A. Hess, *Phys. Rev. A* **1986**, *33*, 3742–3748; b) T. Nakajima, K. Hirao, *Chem. Rev.* **2012**, *112*, 385–402.
[42] E. D. Glendening, J. K. Badenhoop, A. E. Reed, J. E. Carpenter, J. A. Bohmann, C. M. Morales, P. Karafiloglou, C. R. Landis, F. Weinhold, Theoretical Chemistry Institute, University of Wisconsin, Madison, WI, **2018**.
[43] A. D. Becke, *J. Chem. Phys.* **1993**, *98*, 1372–1377.
[44] *Bond Valence Parameters.* http://www.iucr.org/resources/data/datasets/bond-valence-parameters (accessed: 2020.10.03).
[45] a) C. Angeli, R. Cimiraglia, S. Evangelisti, T. Leininger, J. P. Malrieu, *J. Chem. Phys.* **2001**, *114*, 10252–10264; b) C. Angeli, R. Cimiraglia, J.-P. Malrieu, *Chem. Phys. Lett.* **2001**, *350*, 297–305.
[46] M. Atanasov, D. Ganyushin, K. Sivalingam, F. Neese, *Molecular Electronic Structures of Transition Metal Complexes II*, Springer Berlin, Heidelberg, **2011**, pp. 149–220.
[47] R. Boča, *Coord. Chem. Rev.* **2004**, *248*, 757–815.

Manuscript received: May 2, 2023
Accepted manuscript online: July 27, 2023
Version of record online: September 20, 2023